# A DC-Bus Capacitor Discharge Strategy for PMSM Drive System with Large Inertia and Small System Safe Current in EVs

Chao Gong, Yihua Hu, *Senior Member, IEEE,* Guipeng Chen, *Member, IEEE,* Huiqing Wen, *Senior Member, IEEE,* Zheng Wang, *Senior Member, IEEE,* Kai Ni

***Abstract*—When an emergency happens to electric vehicles, the voltage of the DC-bus capacitor, which is an important part of the permanent magnet synchronous machine (PMSM) drive system, requires to be reduced as quickly as possible. Recently, a new idea of directly using the windings to discharge the capacitor has come forth. This paper proposes a physical energy flow model (EFM) to explain explicitly the winding-based discharge mechanism firstly. In the EFM, the performance characteristics of the classical winding-based discharge scheme are evaluated, but it is found that the discharge time will not be qualified when the machine rotor inertia is large and the system safe current is small. In order to reject intense voltage surge, a current control algorithm is proposed to bleed the capacitor voltage. Moreover, the proposed current control method shortens the discharge period to below 3 s for the system studied. The proposed discharge algorithm is verified by the experiment which is conducted on a three-phase PMSM drive system.**

***Index Terms*—Energy flow model, permanent magnet synchronous machine, winding-based discharge, large inertia, system safe current.**

## I. INTRODUCTION

CURRENTLY, permanent magnet synchronous machine (PMSM) drive systems in electric vehicles (EV) are drawing increasing attention due to their excellent characteristics of high efficiency and wide speed regulation range [1]-[10]. Fig.1 shows a commonly used topology of EV PMSM drive system. In addition to a PMSM, there are four other main parts, firstly a battery pack providing energy, then a DC/DC boost converter transferring the low battery voltage into the high voltage that is applied to both the third part, a DC-bus capacitor absorbing high-frequency power surges, and the fourth one, a power inverter [11]-[14]. Once emergency (e.g., car crash) occurs, the system protection device, a circuit interrupter, will be tripped immediately, and the capacitor voltage $U_C$ is supposed to decrease to a safe level $U_{safe}$ (60 V) within 5 s to avoid electrical shock risks according to the United Nation Vehicle Regulation ECE R94 [15].

Generally, all of the transistors in the three-phase inverter will be shut off if a fault or failure is detected [16], [17]. If so, the energy stored in the capacitor cannot be dissipated unless a bleeder circuit in parallel with the capacitor is adopted [18]. This method can definitely meet the requirement that the capacitor discharges quickly, but the use of extra circuits sacrifices the volume, weight and cost of EV drive systems. In order to achieve a cost-effective voltage discharge solution, a brand-new idea of directly using the motor windings to consume the capacitor energy has been presented [11], [19]. This kind of DC-bus capacitor energy consumption method is characterized by directly controlling the *d*, *q*-axis currents in the PMSM to drive the machine to operate normally in spite of emergency situations. In this case, the clutch in the vehicle disconnects the wheels from the traction motor and the motor just rotates with no load [20]. In [19], the DC-bus capacitor voltage is dissipated by applying a constant large *d*-axis current and zero *q*-axis current to the machine. But this discharge algorithm can only be effective when the rotor speed is not higher than the threshold value that is equal to the speed at which the back electromotive force (EMF) of the machine is 60V, otherwise the capacitor recharge phenomenon will be observed because an overcurrent protection mode is triggered when the bus voltage is close to zero as presented in [11], in which the entire voltage discharge process is optimized by three different stages. At the first stage, a nonzero *d*-axis current and zero *q*-axis current are employed to bleed the capacitor voltage. At the instant that the voltage reaches 60 V, the second stage launches and a DC-bus voltage regulation algorithm by applying negative *d*, *q*-axis currents to the PMSM is activated to make the voltage level off until the machine speed is under the threshold $\omega_{mot.th}$. Finally, both *d*, *q*-axis currents will be ramped down to zero and the residual energy is discharged completely. The above-mentioned optimization algorithm has been successfully applied to the high-speed cases when both the

Manuscript received September 07, 2018; revised November 26, 2018; accepted January 18, 2019. *(Corresponding author: Yihua Hu)*.

C. Gong, Y. Hu and K. Ni are with the Department of Electrical Engineering and Electronics, University of Liverpool, Liverpool L69 3GJ, U.K. (E-mail: 1452101806@qq.com, y.hu35@liverpool.ac.uk, k.ni@student.liverpool.ac.uk).

G. Chen is with the School of Aerospace Engineering, Xiamen University, Xiamen 361005, China. (E-mail: cgp2017@xmu.edu.cn).

H. Wen is with the Department of Electrical and Electronic Engineering, Xi'an Jiaotong-Liverpool University, Suzhou 215123, China. (E-mail: Huiqing.Wen@xjtlu.edu.cn).

Z. Wang is with the School of Electrical Engineering, Southeast University, Nanjing 210096, China. (E-mail: zwang@eee.hku.hk).

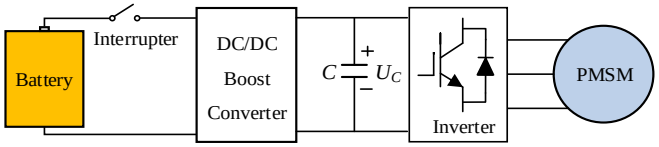


Fig. 1. Topology of EV PMSM drive system.

rotor inertia $J$ of the machine and the system safe current $I_{max}$ are high without capacitor recharge (the red curve in Fig.2).

However, the DC-bus capacitor voltage characteristics are closely related to the system parameters when using the algorithm proposed in [11], especially for the system safe current that neither causes magnet demagnetization nor exceeds the maximum allowable current, and the magnitude of rotor inertia. When $J$ is high but $I_{max}$ is relatively small (eg., $J$=0.24 kg·m$^2$ and $I_{max}$ =100 A), it is difficult to put that optimization method into practice (the blue curve in Fig.2). For the system with large inertia and small safe current, the difficulty in implementing a winding-based discharge algorithm by controlling the $d$, $q$-axis currents is illustrated as follows. The transient discharge capacity is limited and the motor speed declines slowly due to small $I_{max}$. Consequently, the capacitor voltage cannot change, which is shown as the red line in Fig.2, and the discharge time might be over the upper limit. The easiest way to shorten the discharge time is applying a larger $q$-axis but a smaller $d$-axis current to the motor from the outset, by which the motor speed drops quickly. However, a larger negative $q$-axis current will increase the rate of energy conversion from the mechanical energy to the electric one flowing back to the DC-bus side. Therefore, the motor windings are not able to expend the energy synchronously, and a huge voltage surge will emerge inevitably because the capacitance of the DC-bus capacitor is usually not large enough [21]. In order to avoid excessive voltage surge, it is of great importance to figure out how to control the $q$-axis current. Yet there are no studies about the winding-based discharge control algorithms for that kind of system that has large rotor inertia and small system safe current.

This paper proposes a new control method for the PMSM drive system with large inertia and small system safe current to quickly discharge the bus capacitor and safely reduce the motor speed without voltage surge. This method adopts a piecewise $q$-axis current locus and makes full use of the maximum discharge capacity of the system, allowing any active discharge events regardless of the motor speed. In order to illustrate the control algorithm at length, this paper presents an energy flow model (EFM), which is a combination of energetics and electromagnetics. This model is well suited for capturing the transient discharge behaviors of a PMSM drive system, and relying on it, the mechanism and characteristics of both the traditional and novel winding-based discharge schemes are discussed.

The structure of the rest of the paper is as follows. Section II describes an energy flow model (EFM) and presents the mechanism of the winding-based discharge strategies. Section III firstly details the characteristics and also the defects of the published winding-based discharge methods when they are applied to the system with large inertia and small system safe current, and then demonstrates the proposed DC-bus voltage bleeding algorithm. The results of the successful experiments are in Section IV, and Section V presents the conclusion part.

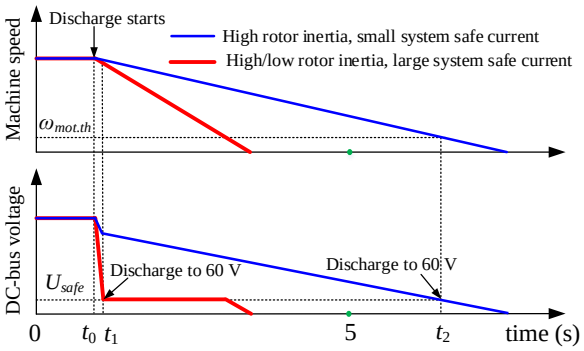


Fig. 2. Discharge characteristics under different system parameters.

## II. Energy Flow Model and Winding-based Discharge Mechanism

Establishing a mathematical or physical model of the drive system is crucial for detailing the winding-based discharge mechanism, illustrating the voltage and current properties, revealing the working status of the motor and designing a novel discharge algorithm for the system with large inertia and small system safe current. Thus, before analyzing the winding-based discharge schemes, the so-called EFM is established.

### A. Energy Flow Model

The EFM used for active discharge is shown in Fig.3. The capacitor is equivalent to a triangular energy tank, and the area of the shaded triangle represents the electric energy packed into the tank. The height of the shaded triangle is equal to the capacitor voltage. $s_1$ and $s_2$ represent two valves whose state can be controlled by $d$, $q$-axis currents. $f_1$ is the energy consumed by mechanical friction. $f_2$ is the kinetic energy of the rotor that is going to be converted into electric energy flowing back to the tank, and most of the energy in the tank ($f_3$) is expended in the form of winding heat loss.

Assume that the active discharge is requested at $t_0$ when the capacitor voltage is $U_{full}$. The initial energy $Q_0$ stored in the tank is as follows:

$$Q_0 = \frac{1}{2} C \cdot U_{full}^{\ 2} \tag{1}$$

where $C$ is the capacitance.

After a period of $\Delta t$, the energy flow can be expressed as:

$$f_1 = \int_{\Delta t} F \cdot \omega_m^{\ 2} dt \tag{2}$$

$$f_2 = \frac{1}{2} J \cdot (\omega_{iq\_st}^{\ 2} - \omega_{iq\_ed}^{\ 2}) - f_1 \tag{3}$$

$$f_3 = \int_{\Delta t} i_d^{\ 2} \cdot R_s dt + \int_{\Delta t} i_q^{\ 2} \cdot R_s dt \tag{4}$$

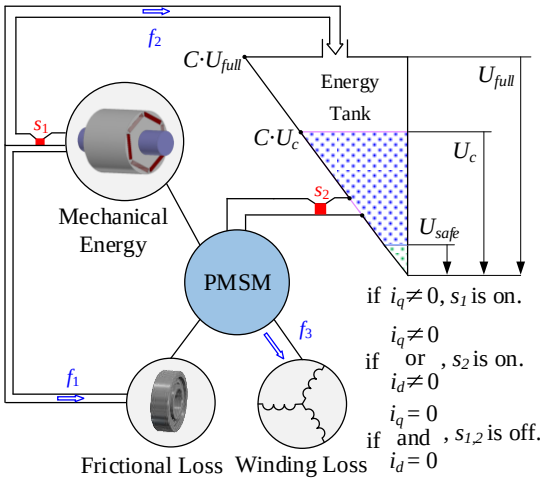


Fig. 3. Energy flow model used for active discharge.

where $\omega_{iq\_st}$ and $\omega_{iq\_ed}$ are the rotor mechanical angular speeds before and after $i_q$ is injected to the machine, respectively. That is, only when $i_q$ is negative could $f_2$ exist. The stator winding resistance is $R_s$, and $F$ is the viscous coefficient. $\omega_m$ represents the instantaneous rotor mechanical angular speed. Then, the remaining energy $Q_{rem}$ in the capacitor is

$$Q_{rem} = Q_0 + f_2 - f_3 \tag{5}$$

The capacitor voltage $U_c$ at the end is

$$U_c = \sqrt{\frac{2 \cdot Q_{rem}}{C}} \tag{6}$$

The above is the energetic part of the proposed EFM, which is based on the law of the conservation of energy. However, that is not enough for accurately evaluating the transient performance characteristics of the drive system and calculating the amount of energy conversion. To complement the deficiency, an electromagnetic part is added to the EFM [22]-[25]:

$$\frac{di_d}{dt} = -\frac{R_s}{L_d} i_d + \frac{L_q}{L_d} p\omega_m i_q + \frac{u_d}{L_d} \tag{7}$$

$$\frac{di_q}{dt} = -\frac{L_d}{L_q} p\omega_m i_d - \frac{R_s}{L_q} i_q + \frac{u_q}{L_q} - \frac{\Psi_f}{L_q} p\omega_m \tag{8}$$

$$\frac{d\omega_m}{dt} = \frac{1}{J}(1.5p(\Psi_f i_q + (L_d - L_q) i_d i_q) - F\omega_m) \tag{9}$$

where $u_d$, $u_q$ are $d$, $q$-axis control voltages. $L_d$, $L_q$ are $d$, $q$-axis inductances. Additionally, $p$ represents the number of machine pole pairs and $\psi_f$ is the permanent magnet flux linkage.

### *B. Winding-based Discharge Mechanism*

The winding-based discharge mechanism includes, firstly, the winding resistance, which functions as a bleeder load. Specifically, an external emergency does not trigger the protection regime immediately. Instead, an active discharge operating mode by using the windings to consume the energy stored in the capacitor launches prior to it. Although that process is able to bring down the capacitor voltage, it is highly required to shorten the discharge period as much as possible (5 s is long in this aspect), so as to shut down the entire drive system in time. Besides, according to the different states of $s_1$ and $s_2$ (directly related to $i_d$ and $i_q$) in Fig.3, the discharge mechanism can be expressed as four basic cases shown in Table I.

TABLE I
MECHANISM OF WINDING-BASED DISCHARGE SCHEMES

| Current states | | Valve status | | Proportion of energy flow | | |
|---|---|---|---|---|---|---|
| $i_d$ | $i_q$ | $s_1$ | $s_2$ | $f_1$ | $f_2$ | $f_3$ |
| zero | zero | off | off | large | zero | zero |
| nonzero | zero | off | on | large | zero | nonzero |
| zero | nonzero | on | on | small | nonzero | nonzero |
| nonzero | nonzero | on | on | small | nonzero | nonzero |

*a*) When both $i_q$ and $i_d$ are zero, $s_1$ and $s_2$ are off. There is only one path to consume the rotor kinetic energy by $f_1$, while the electric energy in the tank cannot flow out. Namely, $f_2$=$f_3$=0. The capacitor voltage remains at the maximum level $U_{full}$. In this case, the discharge time will be very long since the PMSM may be freely spinning (multiple minutes in duration).

*b*) When $i_q$ is kept at zero and $i_d$ is negative, $s_1$ is off but $s_2$ is on. The rotor mechanical energy cannot be converted into electric energy, and it is consumed only by friction, but the energy stored in the tank can be rapidly radiated because of the existence of windings ($f_2$=0, $f_3$≠0).

*c*) When $i_q$ is nonzero and $i_d$ is zero, both $s_1$ and $s_2$ are on. Most of the rotor mechanical energy will be transformed into capacitor electric energy, and then consumed by the windings together with the initial energy in the tank ($f_2$≠0, $f_3$≠0). At the same time, a small percentage of kinetic energy is consumed by the path of $f_1$.

*d*) When negative $i_q$ and $i_d$ are injected into the machine, $s_1$ and $s_2$ are in open states. A large amount of rotor mechanical energy floods into the tank ($f_2$≠0, $f_3$≠0) but the capacitor energy is dissipated by $f_3$ very quickly.

A classic winding-based discharge process always contains one or more of the aforementioned cases. In [19], only the case *b*) is tried out to achieve the bus capacitor voltage discharge. From the very beginning to the end, the *d*-axis reference current is set as the safe current ($I_{max}$) of system, and the *q*-axis reference current is zero. In [11], the discharge process is divided into three phases, the first of which employs case *b*), and both the second and the third of which adopt case *d*) by applying nonzero *d*, *q*-axis currents to the machine. The proposed method in this paper only utilizes the fourth case *d*), which will be detailed in Section III.

## III. Winding-based Discharge Approaches Applied to the System with Large Inertia and Small Safe Current

For the purpose of redesigning an effective and high-efficiency discharge approach, it is significant to discover beforehand the characteristics and defects of the traditional winding-based bleeding schemes. In virtue of the EFM, the diverse characteristics of different discharge methods are analyzed and a novel algorithm based on direct current control is presented in this section.

In order to implement an intuitive discussion on the winding-based discharge strategies, a PMSM drive system for

TABLE II
PMSM DRIVE SYSTEM PARAMETERS

| Parameter | Value | Unit |
|---|---|---|
| stator winding resistance $R_s$ | 0.275 | Ω |
| $d$-axis inductance $L_d$ | 0.8 | mH |
| $q$-axis inductance $L_q$ | 0.8 | mH |
| the number of pole pairs $p$ | 3 | - |
| moment of inertia $J$ | 0.24 | kg·m$^2$ |
| viscous coefficient $F$ | 0.0035 | - |
| permanent magnet flux linkage $\Psi_f$ | 0.18 | Wb |
| DC-bus voltage $V_{DC\text{-}bus}$ | 310 | V |
| system safe current $I_{max}$ | 100 | A |
| rated speed $\omega_{rated}$ | 345 | rad/s |
| DC-bus capacitor $C$ | 560 | μF |

EV with parameters in Table II is studied. The active discharge starts when the motor speed is at the rated value $\omega_{rated}$.

### *A. Discharge Characteristics and Defects of Traditional Winding-based Discharge Schemes*

When the bleeding algorithm in [19] (traditional method *a*) is applied to the system with large inertia and small safe current, the initial DC-bus voltage is promptly reduced. But it cannot drop under the safe level as quickly as expected so that the capacitor is charged when the back EMF is higher than the DC-bus capacitor voltage, slowing the discharge rate. The simulation results of capacitor voltage and speed characteristics in Fig.4 (a) proved the above statement. The discharge is requested at 0.5 s when -100 A *d*-axis and zero *q*-axis currents are utilized. The capacitor voltage immediately jumped down to 170 V, after which it declines slowly and reaches the safe value until 5.5 s (the discharge time is 5.0 s) when the speed reaches 98 rad/s. The reason why the capacitor voltage can only decrease to 170 V in the rapid discharge process, instead of decreasing to under 60 V as desired is that the highest allowable current of this system is so low that the instantaneous discharge capacity is limited. In detail, when the negative $i_d$ (-100 A) is applied, the air-gap field of the motor is weakened instantly, reducing the back EMF simultaneously to about 170 V at the rated speed. At the moment, the capacitor voltage is much higher than the back EMF, so that the energy can flow in one direction from the capacitor to PMSM. But soon the capacitor voltage will not be constantly higher than the back EMF due to the gradually declining rotor speed. Afterwards, the capacitor will be in a state of discharge accompanied by charge (slow discharge), and only when the rotor speed goes down to the position where the back EMF is equal to $U_{safe}$ will the capacitor voltage remain under 60 V.

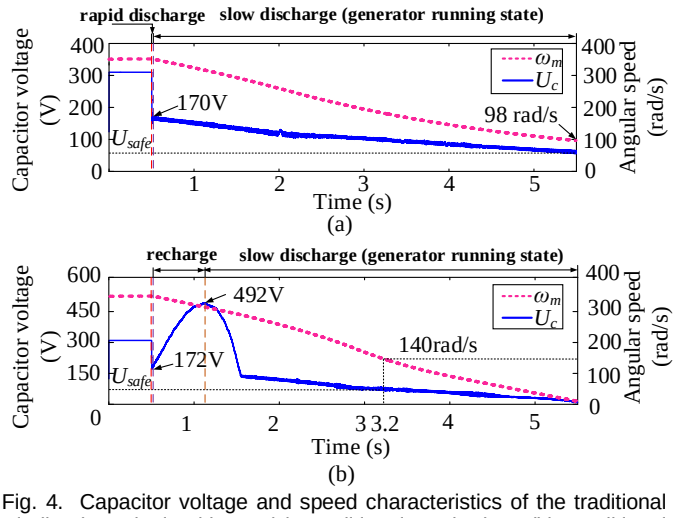


Fig. 4. Capacitor voltage and speed characteristics of the traditional winding-based algorithms. (a) Traditional method *a*. (b) Traditional method *b*.

The above-mentioned voltage and speed characteristics of the traditional method *a* also indicate that the first stage of the algorithm in [11] cannot be achieved, not to mention then stabilizing the voltage at a value slightly under $U_{safe}$. Hence, it is impracticable to directly apply that current control algorithm to the system with large inertia and small safe current. But in order to shorten the discharge time in Fig.4 (a), we can learn from the second stage of the discharge algorithm in [11], solving the problem by controlling the *q*-axis current to keep at a higher level (traditional method *b*) so as to speed up the deceleration process. Fig.4 (b) illustrates the simulation results of the process. In this situation, the *d*-axis of (-98 A) and *q*-axis current of (-20 A) are adopted as the reference values at 0.5 s. Compared to Fig.4 (a), the DC-bus voltage reaches 60 V more quickly within 3.2 s (the discharge time is 2.7 s) when the speed arrives at about 140 rad/s. However, there is an obvious voltage surge in a short period after the beginning of discharge, and if the reference value of $i_q$ is increased, the peak of the voltage surge will get higher. This happens because a larger negative *q*-axis current can increase the energy conversion rate from the mechanical energy to electric energy, which is more significant when the machine speed is high, but the windings are not able to expend the energy synchronously because the total discharge current does not increase.

The current characteristics of the traditional winding-based algorithms are compared in Fig.5 where two interesting phenomena can be seen. Firstly, the *q*-axis current in the windings turns to be negative passively without following the planned trajectory for the method *a*, which seems to correspond to case *d*), but $i_q$ is actively generated in the system rather than being passively injected as in the method *b*. Secondly, the discharge current, especially the *d*-axis current, will witness an downward trend when the DC-bus voltage is not large enough to maintain it at the reference level for both methods. At the time, the energy consumption rate by the machine windings

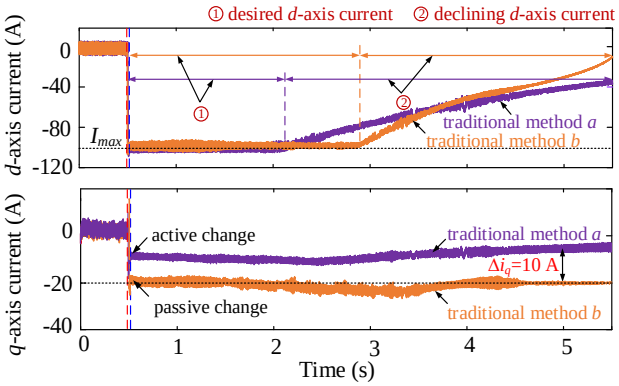


Fig. 5. *d*,*q*-axis current characteristics of the traditional winding-based algorithms.

goes down at the same time. Therefore, another effective way to shorten the discharge time is to extend the duration of applying a larger discharge current. Apart from faster deceleration, it is also in that way for the method *b* to achieve a shorter discharge period. In detail, firstly, even though $i_d$ falls just by about 2 A (2%), it lasts 0.8 s longer at the desired position before declining. Secondly, $i_q$ can remain at nearly -20 A during the whole process, and only when the bus voltage reduces almost to zero will it decline in method *b*. Comparatively, the *q*-axis current generated in method *a* is lower ($\triangle i_q$) and experiences a declining trend from 2.5 s.

In terms of the defects, the discharge time for the traditional method *a* is not qualified. Although the traditional method *b* shows more attractive characteristic from this aspect, namely shorter discharge time, the voltage recovery is unwanted for the sake of system safety. As a consequence, Section III-*B* will explain a novel DC-bus capacitor discharge strategy by calculating and applying appropriate *q*-axis reference currents to shorten the discharge period, and meanwhile avoiding voltage rise effectively.

### *B. Proposed Discharge Algorithm*

By comparing the bleeding properties of the above two algorithms, it is feasible to shorten the overall bleeding time by using a relatively high *q*-axis reference current $i_{q\_ref}$. However, it is also found that when the *q*-axis current in the machine is about -10 A from the beginning, there is no voltage rise phenomenon. But when it is controlled at -20 A, the voltage surge shows up in the high speed range. So the locus of $i_{q\_ref}$ should be well designed if a high *q*-axis current control strategy is employed to shorten the discharge time as well as eliminate the voltage surge. Now, a new issue of how to determine the reference signal arises.

When the negative reference $i_{q\_ref}$ and *d*-axis reference current $i_{d\_ref}$ keep fixed, a constant electromagnetic braking torque $T_e$ will be produced once the currents in the PMSM are controlled to track the reference values.

$$\begin{aligned} T_e &= 1.5p(\Psi_f i_q + (L_d - L_q) i_d i_q) \\ &= 1.5p(\Psi_f i_{q\_ref} + (L_d - L_q) i_{d\_ref} i_{q\_ref}) \end{aligned} \tag{10}$$

Ignoring the term of reluctance torque for simplicity, $T_e$ can be expressed as:

$$T_e = 1.5 p \Psi_f i_{q\_ref} \tag{11}$$

So the motor will slow down with a constant deceleration $a_{dec}$.

$$a_{dec} = \frac{|T_e|}{J} = \frac{1.5}{J} p \Psi_f i_{q\_ref} \tag{12}$$

After a period of $\triangle t$, the kinetic energy converted into the electric energy $f_2$ in (3) can be rewritten as:

$$f_2 = 1.5 p \Psi_f i_{q\_ref} \Delta t \omega_{iq\_st} - \frac{9}{8J} (p \Psi_f i_{q\_ref})^2 \Delta t^2 - f_1 \tag{13}$$

Therefore, $f_2$ is proportional to the machine speed if a constant *q*-axis current is adopted. Thus, the case that the energy conversion rate (from mechanical energy to electric energy) is high but the windings cannot consume the energy synchronously ($f_2 > f_3$) happens only in the high speed range. The problem can be solved by employing piecewise *q*-axis current as in Fig.6. The entire discharge process is divided into several periods of $\triangle t$. $i_{q\_ref}$ is smaller when the speed is high, and gets larger and larger over time. On the basis of EFM, the key technique proposed in this paper to avoid the voltage surge can be described as letting $f_2 \le f_3$ over each period of $\triangle t$. In other words, the phenomenon will vanish whenever the mechanical energy conversion rate is not higher than the energy consumption rate. The computing method for $i_{q\_refi}$ is shown below.

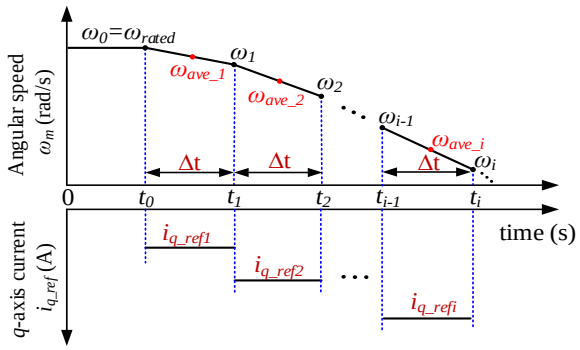


Fig. 6. *q*-axis reference current and desired speed characteristics in the entire discharge process.

In this paper, we try to ensure the maximum capacity of discharge, so the system current is expected to be controlled to maintain at $I_{max}$ during the whole process, that is,

$$i_{d\_ref}^2 + i_{q\_ref}^2 = I_{max}^2 \tag{14}$$

Take the *i*th interval as an example, on the basis of the formulas (4) and (10),

$$f_3 = I_{max}^2 \cdot R_s \cdot \Delta t \tag{15}$$

$f_2$ is also equal to the work done by the braking torque, namely,

$$f_2 = \int_{\Delta t} |T_e| \cdot \omega_m dt \tag{16}$$

When $\triangle t$ is short, the angular speed $\omega_m$ can be approximated as the average value $\omega_{ave\_i}$ from $t_{i-1}$ to $t_i$. So $f_2$ can be rewritten as:

$$f_2 = |T_e| \cdot \omega_{ave\_i} \cdot \Delta t \tag{17}$$

$$\omega_{ave\_i} = \frac{\omega_{i-1} + \omega_i}{2} \tag{18}$$

$\omega_0$ is the initial speed when discharge is requested. In order to calculate $\omega_i$, assume that the mechanical friction torque is much smaller than $T_e$ and ignore its influence on the deceleration. $\omega_i$ can be expressed as:

$$\omega_i = \omega_{i-1} + a_{dec} \cdot \Delta t \tag{19}$$

According to the requirement $f_2 \le f_3$ and (12), $i_{q\_refi}$ can be calculated then, that is:

$$i_{q\_ref\,i} \ge \frac{-\omega_{i-1} + \sqrt{\omega_{i-1}^2 - \frac{2\Delta t}{J} I_{max}^2 R_s}}{\frac{1.5 p \Psi_f \Delta t}{J}} \tag{20}$$

Substitute (20) into (14), a piecewise *d*-axis reference current locus can be derived as:

$$i_{d\_refi} = \sqrt{I_{max}^2 - i_{q\_refi}^2} \tag{21}$$

For the purpose of reducing the motor speed as quickly as possible, the absolute value of $i_{q\_refi}$ needs to be maximum

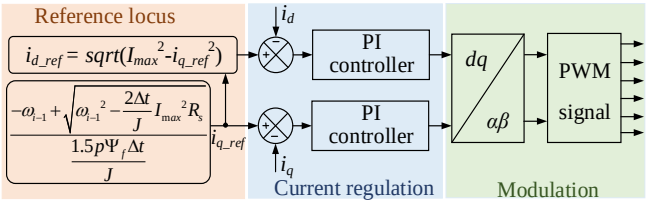


Fig. 7. Block diagram of the proposed discharge.

within the permissible range. Fig.7 illustrates the block diagram of the discharge method. Two current controllers and a pulse width modulation (PWM) signal generator are adopted in the topology for discharge.

Besides, it should be acknowledged that the shorter $\Delta t$ is, the more representative and typical $\omega_{ave\_i}$ will be. Assume that the change of the machine parameters can be ignored during discharge process and when $\Delta t$ is set as 0.5 s and $\omega_0=\omega_{rated}$, Fig.8 shows the values of $i_{d\_ref}$ and $i_{q\_ref}$ for the different intervals and the corresponding simulation results. In comparison with the method *a*, firstly, the capacitor voltage falls to 60 V within 3.7 s (discharge time is 3.2 s) when the speed gets to about 110 rad/s for the novel method, which becomes shorter and satisfies the discharge requirement. The reason why the threshold speed for the novel method is higher than that for traditional method *a* (but lower than traditional method *b*) is that the back-EMF of the machine is affected by the flux-weakening *d*-axis current. The larger the negative $i_d$ is, the higher level the rotor speed should stand at for obtaining the same voltage. Secondly, the *q*-axis current in the motor can track the reference values well and the *d*-axis current starts to decline from about 2.5 s, proving that the new current control algorithm is capable of extending the duration of applying relatively large discharge currents to the machine. Then, the voltage surge phenomenon is completely avoided, contributing to eliminating the electrical shock risks of the EV powertrains. Finally, an interesting phenomenon is that the current references are derived by setting $f_2=f_3$ but the bus voltage continues to drop during discharge. This happens because firstly, the energy consumed by friction ($f_1$) is ignored when

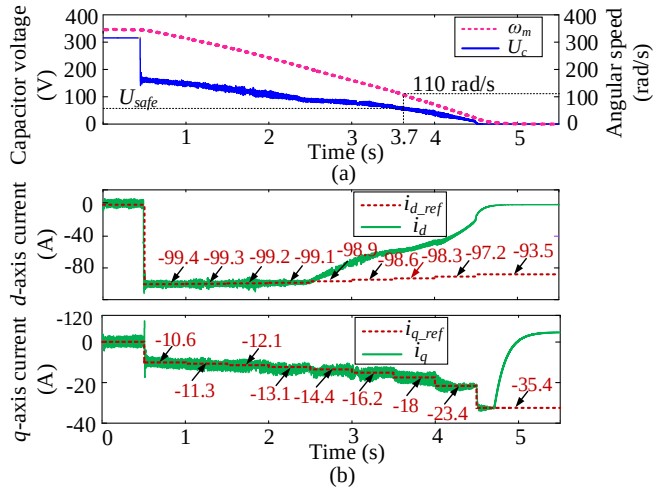


Fig. 8. Characteristics of the proposed winding-based algorithm. (a) Capacitor voltage and PMSM mechanical angular speed. (b) *d*,*q*-axis current.

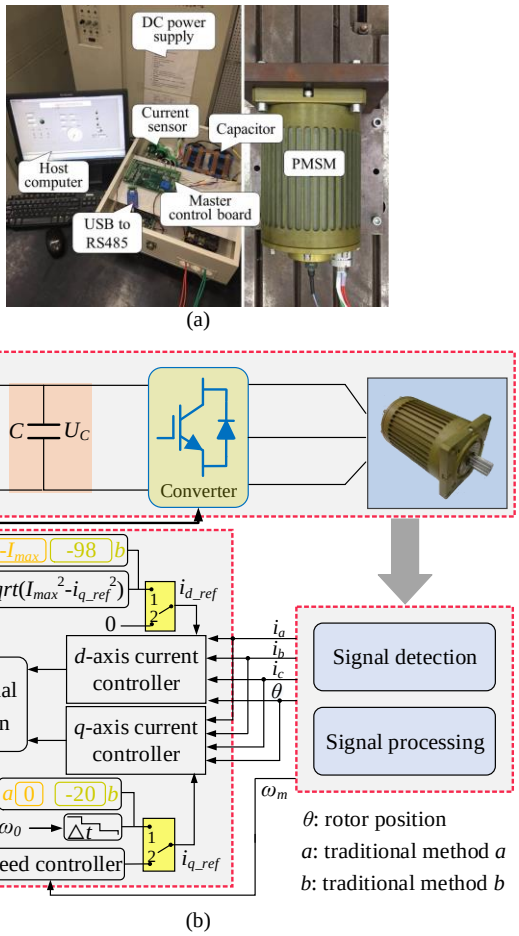


Fig. 9. Experimental system. (a) Photo of the experimental setup. (b) Schematic diagram.

designing the current reference locus. Considering that the mechanical friction can expend energy, the capacitor voltage will decline. Secondly, it can be noticed that at the start of each period in Fig.8 (b), there exist current overshoots of the real $i_q$. This will cause that the speed declines faster over the former half period of $\triangle t$ than that of the latter half period. Consequently, the calculated $f_2$ is smaller than the real value, which will in turn lead to that the calculated *q*-axis reference current is relatively lower. Thus, although we expect that $f_2 = f_3$, $f_2$ is less than $f_3$ in reality. But the goal to avoid voltage surge can be achieved. The characteristics of the proposed winding-based method will also be verified by experiments in Section IV.

## IV. Experimental Results

Experiments are conducted on a three-phase PMSM whose parameters are also consistent with Table II. The experimental equipment is shown in Fig.9 (a). A DC power supply is available at 310 V. An intelligent power module (IPM), Mitsubishi PM100RLA120, is used as the voltage source inverter with the frequency of 10 kHz. Four thin-film capacitors, DHF DAWNCAP 140 μF, are connected in parallel to compose the desired 560 μF DC-bus capacitor. The proposed discharge algorithm is implemented on DSP TMS320F28335 controller board. The real rotor position is detected by a rotary

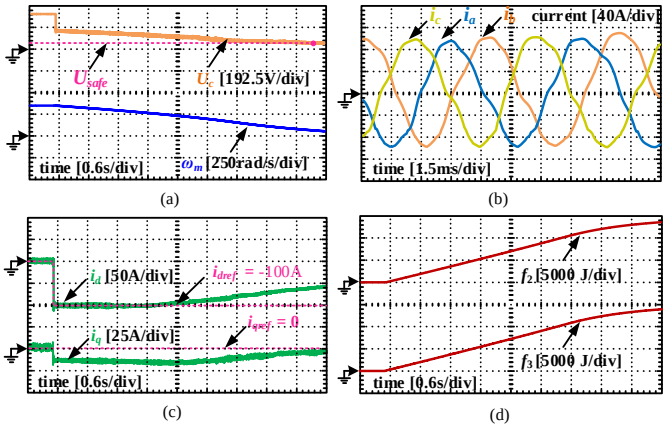


Fig. 10. Experimental results of the traditional discharge method *a* when emergency occurs at the speed of 345 rad/s. (a) DC-bus capacitor voltage and machine speed. (b) Phase current. (c) *d*,*q*-axis current. (d) Amount of energy conversion and consumption by windings.

transformer. Hall current sensors, HNC-100LT, are used to measure three-phase currents while the motor *d*, *q*-axis currents are calculated by the digital controller. The DC-bus voltage is measured by a voltage transducer LV25-P. Using the USB-RS485 communication interface, the collected data are transmitted to and further recorded by the host computer. The schematic diagram of the traditional and proposed discharge methods is presented in Fig.9 (b). A programmatic virtual switch is used to select the operating state of the system. When the system works normally, port 2 is connected and the system can be controlled by any PMSM drive technique, such as double closed-loop speed regulation strategy [26] and direct torque control method [27]. Once an emergency occurs, port 1 is connected and the winding-based discharge algorithm is implemented.

Assume the active discharge request occurs at 0.5 s when the motor speed is $\omega_{rated}$. Fig.10 (a) illustrates that the capacitor voltage of the traditional method *a* drops to the safe level at nearly 5.75 s, being a little bit longer than that in the simulation result. Fig.10 (b) and (c) show the characteristics of the three phase currents from 0.52 to 0.5215s and the *d*, *q*-axis currents, respectively. Before 2.4 s, the *d*-axis current can track the prescribed trajectory well, after which it goes down gradually. In accordance with the simulation results, the *q*-axis current

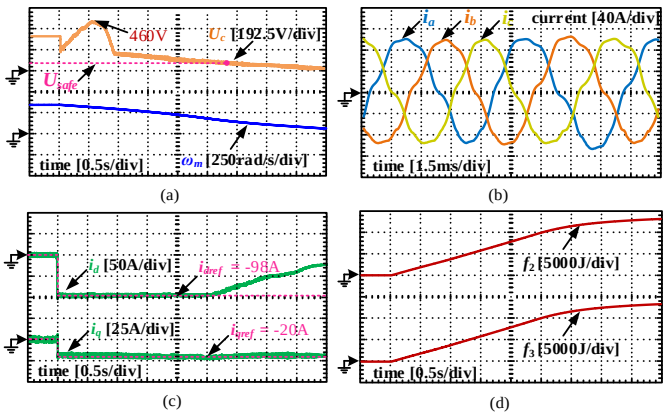


Fig. 11. Experimental results of the traditional discharge method *b* when emergency occurs at the speed of 345 rad/s. (a) DC-bus capacitor voltage and machine speed. (b) Phase current. (c) *d*,*q*-axis current. (d) Amount of energy conversion and consumption by windings.

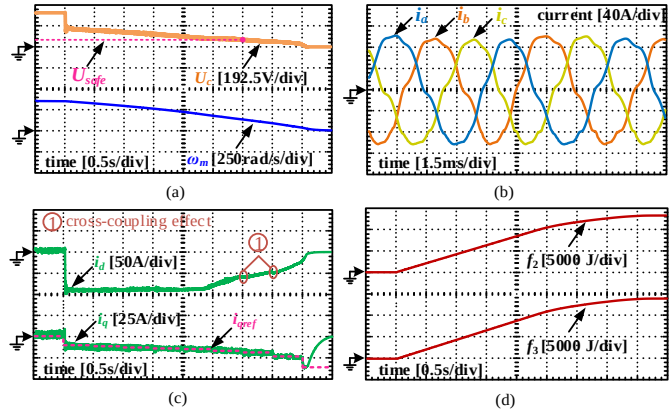


Fig. 12. Experimental results of the proposed discharge algorithm when emergency occurs at the speed of 345 rad/s. (a) DC-bus capacitor voltage and machine speed. (b) Phase current. (c) *d*,*q*-axis current. (d) Amount of energy conversion and consumption by windings.

(about 14 A) is generated automatically at the time when the discharge is requested, while it starts to decline from 2.5 s and reaches below -5 A at 6.0 s. Additionally, $f_2$ and $f_3$ can be calculated according to the EFM, and Fig.10 (d) demonstrates that about 14000 J of mechanical energy is converted into the electric energy and then consumed by the windings by the end of discharge.

Fig.11 depicts the discharge characteristics of the traditional discharge method *b*. The discharge time is 2.8 s, which is very close to that in the simulation result in Fig.4 (b). However, a marked voltage surge (about 460 V) appears in the high speed range. In terms of the current characteristics, $i_q$ can stay at the desired value during the whole process while $i_d$ witnesses an downward trend from 3.1 s. Similar to method *a*, a total of approximately 14000 J of energy is expended by the windings during the whole process.

Fig.12 demonstrates the experimental results of the proposed bleeding algorithm. Overall, it can be noticed that the DC-bus capacitor voltage drops to 60 V at nearly 3.5 s and the voltage surge disappears. The reason why the proposed algorithm can avoid remarkable voltage surge in the PMSM drive system with large inertia is that a piecewise *q*-axis current locus is used. The higher the mechanical speed is, the relatively lower $i_q$ is applied to the machine, as shown in Fig.12 (c), producing smaller braking electromagnetic torque. Consequently, the motor speed

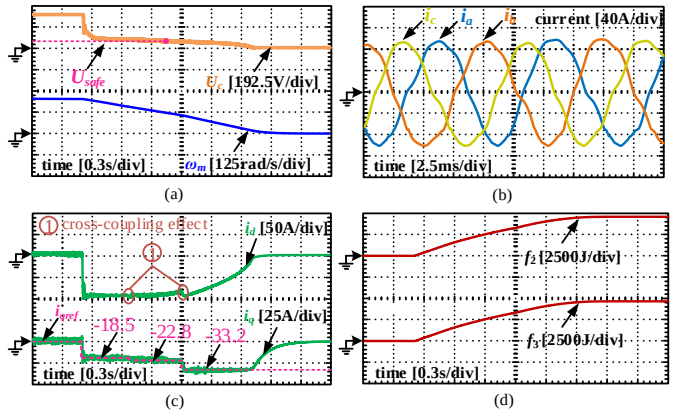


Fig. 13. Experimental results of the proposed discharge algorithm when emergency occurs at the speed of 200 rad/s. (a) DC-bus capacitor voltage and machine speed. (b) Phase current. (c) *d*,*q*-axis current. (d) Amount of energy conversion and consumption by windings.

TABLE III
FEATURES OF DC-BUS VOLTAGE BLEEDING ALGORITHMS

| Type of algorithm | Discharge time (s) | Voltage surge (V) |
|---|---|---|
| Traditional method *a* | 5.25 | none |
| Traditional method *b* | 2.8 | 460 |
| Proposed method | 3.0 | none |

declines more slowly in the high speed range, making it possible that the energy consumption rate by windings is no lower than the mechanical energy conversion rate. That stands in contrast with Fig.11 (c) in which $i_q$ always keeps at a high position and the motor windings are incapable of consuming the converted mechanical energy synchronously. Before leaving Fig.12 (c), we find that the *d*-axis current begins to fall from 2.8 s, proving the statement that the new algorithm can extend the duration of applying relatively large discharge current to the motor compared to method *a*.

Table III shows the features of all the three above-mentioned bus voltage bleeding algorithms when they are applied to a drive system with large rotor inertia and small safe current. As far as the proposed method is concerned, although the discharge time is about 3.0 s, which is a little bit longer than 2.8 s for method *b*, it has been shortened greatly by 42.8% compared to that in the traditional strategy *a*. More importantly, the large voltage surge disappears. This is crucial to strengthen the security of both the EV components and passengers, especially in an emergency.

In order to verify that the proposed algorithm is effective regardless of the machine speed, as shown in Fig.13, the experiment was carried out when assuming an active discharge is requested at the speed of 200 rad/s. For the sake of low initial speed, the calculated *q*-axis reference current gets lower (-18.5 A) at first. The DC-bus voltage descends to the safe level at about 1.35s and no large voltage recovery is witnessed. Only about 4500 J of kinetic energy is transferred to electric energy and consumed by the machine windings when the rotor speed arrives at zero.

Looking at the current properties in Fig.12 (c) and Fig.13 (c) in detail, the *d*-axis current fluctuates at the moment when a larger *q*-axis current is applied to the machine in the proposed algorithm. This phenomenon arises from the cross-coupling effect [28]-[30]. Besides, the *q*-axis current can level off at the desired value until the DC-bus voltage is nearly zero, while the *d*-axis current starts to decline in advance in accord with the simulation results. That indicates that the *d*-axis current is more sensitive to the declining DC-bus voltage in the machine when a winding-based bleeding algorithm is employed. Therefore, a nonzero *q*-axis current control algorithm is more suitable for bleeding the DC-bus voltage.

## V. Conclusion

It is cost-effective to directly use PMSM windings rather than external bleeder circuits for discharging the DC-bus capacitor energy, and several winding-based discharge methods emerged. However, they are not effective when the drive system has large rotor inertia and small safe current.

In the first place, this paper proposes an EFM model, which is a combination of energetics and electromagnetics, and it is utilized to illustrate the mechanism of the traditional winding-based discharge algorithms and performance characteristics in the process of bleeding. Secondly, aiming at the system with large rotor inertia and low safe current, this research analyzes the defects of the traditional methods and proposes a segmented nonzero *d*, *q*-axis current control algorithm, avoiding large voltage surge and shortening the discharge time simultaneously. The simulation and experimental results prove that the proposed current control algorithm is more suitable for bleeding the capacitor voltage of the PMSM drive systems with large inertia and small system safe current in EVs compared to the traditional methods. In conclusion, the proposed winding-based discharge approach can avoid voltage breakdown hazard if an emergency occurs, improving the safety of the EV traction systems regardless of the system parameters, especially the maximum allowable current and rotor inertia of the traction PMSM.

## References


[1] M. Chen and J. Lu, "High-Precision Motion Control for a Linear Permanent Magnet Iron Core Synchronous Motor Drive in Position Platform, " in *IEEE Transactions on Industrial Informatics*, vol. 10, no. 1, pp. 99-108, Feb. 2014.

[2] J. Lara, J. Xu and A. Chandra, "Effects of Rotor Position Error in the Performance of Field-Oriented-Controlled PMSM Drives for Electric Vehicle Traction Applications," in *IEEE Transactions on Industrial Electronics*, vol. 63, no. 8, pp. 4738-4751, Aug. 2016.

[3] J. Lu, X. Zhang, Y. Hu, J. Liu, C. Gan and Z. Wang, "Independent Phase Current Reconstruction Strategy for IPMSM Sensorless Control Without Using Null Switching States," in *IEEE Transactions on Industrial Electronics*, vol. 65, no. 6, pp. 4492-4502, June 2018.

[4] P. L. Xu and Z. Q. Zhu, "Novel Carrier Signal Injection Method Using Zero-Sequence Voltage for Sensorless Control of PMSM Drives," in *IEEE Transactions on Industrial Electronics*, vol. 63, no. 4, pp. 2053-2061, April 2016.

[5] R. Ni, D. Xu, F. Blaabjerg, K. Lu, G. Wang and G. Zhang, "Square-Wave Voltage Injection Algorithm for PMSM Position Sensorless Control With High Robustness to Voltage Errors," in *IEEE Transactions on Power Electronics*, vol. 32, no. 7, pp. 5425-5437, July 2017.

[6] G. Feng, C. Lai, K. L. V. Iyer and N. C. Kar, "Improved High-Frequency Voltage Injection Based Permanent Magnet Temperature Estimation for PMSM Condition Monitoring for EV Applications," in *IEEE Transactions on Vehicular Technology*, vol. 67, no. 1, pp. 216-225, Jan. 2018.

[7] Y. Mao, J. Yang, T. Wang, D. Yin and Y. Chen, "High dynamic sensorless control for PMSMs based on decoupling adaptive observer," *2016 IEEE Energy Conversion Congress and Exposition*, Milwaukee, WI, 2016, pp. 1-8.

[8] T. Wang, C. Liu, G. Lei, Y. Guo and J. Zhu, "Model predictive direct torque control of permanent magnet synchronous motors with extended set of voltage space vectors," in *IET Electric Power Applications*, vol. 11, no. 8, pp. 1376-1382, Sep. 2017.

[9] H. Zhu, X. Xiao and Y. Li, "Torque Ripple Reduction of the Torque Predictive Control Scheme for Permanent-Magnet Synchronous Motors," in *IEEE Transactions on Industrial Electronics*, vol. 59, no. 2, pp. 871-877, Feb. 2012.

[10] F. Mwasilu and J. W. Jung, "Enhanced Fault-Tolerant Control of Interior PMSMs Based on an Adaptive EKF for EV Traction Applications," in *IEEE Transactions on Power Electronics*, vol. 31, no. 8, pp. 5746-5758, Aug. 2016.

[11] Z. Ke, J. Zhang and M. W. Degner, "DC Bus Capacitor Discharge of Permanent-Magnet Synchronous Machine Drive Systems for Hybrid Electric Vehicles," in *IEEE Transactions on Industry Applications*, vol. 53, no. 2, pp. 1399-1405, March-April 2017.

[12] J. Zheng, Z. Wang, D. Wang, Y. Li and M. Li, "Review of fault diagnosis of PMSM drive system in electric vehicles," *2017 36th Chinese Control Conference*, Dalian, 2017, pp. 7426-7432.

[13] P. Dost and C. Sourkounis, "On Influence of Non Deterministic Modulation Schemes on a Drive Train System With a PMSM Within an Electric Vehicle," in *IEEE Transactions on Industry Applications*, vol. 52, no. 4, pp. 3388-3397, July-Aug. 2016.

[14] A. Choudhury, P. Pillay and S. S. Williamson, "DC-Link Voltage Balancing for a Three-Level Electric Vehicle Traction Inverter Using an Innovative Switching Sequence Control Scheme," in *IEEE Journal of Emerging and Selected Topics in Power Electronics*, vol. 2, no. 2, pp. 296-307, June 2014.
[15] United Nation Economic Commission for Europe Vehicle Regulation, No.94 (ECE R94), Unifrom provisions concerning the approval of vehicles with regard to the protection of the occupants in the event of a frontal collision, Rev. 2, Annex 11, Aug. 2013.
[16] Chao Gong, Jinglin Liu, Zexiu Han and Haozheng Yu, "Analysis on uncontrolled generation in electrical vehicles and a battery protection method," *2017 IEEE 3rd International Future Energy Electronics Conference and ECCE Asia*, Kaohsiung, 2017, pp. 1606-1610.
[17] Y. Zhang and T. M. Jahns, "Uncontrolled Generator Operation of PM Synchronous Machine Drive With Current-Source Inverter Using Normally on Switches," in *IEEE Transactions on Industry Applications*, vol. 53, no. 1, pp. 203-211, Jan.-Feb. 2017.
[18] A. K. Kaviani, B. Hadley and B. Mirafzal, "A Time-Coordination Approach for Regenerative Energy Saving in Multiaxis Motor-Drive Systems," in *IEEE Transactions on Power Electronics*, vol. 27, no. 2, pp. 931-941, Feb. 2012.
[19] T. Goldammer, T. Le, J. Miller, and J. Wai, "Active high voltage bus bleed down," U.S. Patent 20120161679 A1, Jun. 28, 2012.
[20] T S. Ashida, K. Yamada, M. Nakamura, T. Shimana, and T. Soma, "Electric vehicle, and control apparatus and control method for electric vehicle," U.S.Patent 8631894 B2, Jan. 21, 2014.
[21] G. J. Su and L. Tang, "A segmented traction drive system with a small dc bus capacitor," *2012 IEEE Energy Conversion Congress and Exposition*, Raleigh, NC, 2012, pp. 2847-2853.
[22] Z. Mynar, L. Vesely and P. Vaclavek, "PMSM Model Predictive Control With Field-Weakening Implementation," in *IEEE Transactions on Industrial Electronics*, vol. 63, no. 8, pp. 5156-5166, Aug. 2016.
[23] T. Tarczewski and L. M. Grzesiak, "Constrained State Feedback Speed Control of PMSM Based on Model Predictive Approach," in *IEEE Transactions on Industrial Electronics*, vol. 63, no. 6, pp. 3867-3875, June 2016.
[24] J. Linares-Flores, C. García-Rodríguez, H. Sira-Ramírez and O. D. Ramírez-Cárdenas, "Robust Backstepping Tracking Controller for Low-Speed PMSM Positioning System: Design, Analysis, and Implementation," in *IEEE Transactions on Industrial Informatics*, vol. 11, no. 5, pp. 1130-1141, Oct. 2015.
[25] G. Feng, C. Lai and N. C. Kar, "Particle-Filter-Based Magnet Flux Linkage Estimation for PMSM Magnet Condition Monitoring Using Harmonics in Machine Speed," in *IEEE Transactions on Industrial Informatics*, vol. 13, no. 3, pp. 1280-1290, June 2017.
[26] L. Sun, X. Wang, Z. Deng and Q. Ding, "Research on stable regions of double-closed loop system for PMSM with low-pass filters, " *2014 17th International Conference on Electrical Machines and Systems*, Hangzhou, 2014, pp. 1150-1156.
[27] F. Niu, B. Wang, A. S. Babel, K. Li and E. G. Strangas, "Comparative Evaluation of Direct Torque Control Strategies for Permanent Magnet Synchronous Machines," in *IEEE Transactions on Power Electronics*, vol. 31, no. 2, pp. 1408-1424, Feb. 2016.
[28] A. Rabiei, T. Thiringer, M. Alatalo and E. A. Grunditz, "Improved Maximum-Torque-Per-Ampere Algorithm Accounting for Core Saturation, Cross-Coupling Effect, and Temperature for a PMSM Intended for Vehicular Applications," in *IEEE Transactions on Transportation Electrification*, vol. 2, no. 2, pp. 150-159, June 2016.
[29] Xiaochun Fang, Fei Lin and Zhongping Yang, "A modified flux-weakening control method of PMSM based on the d-q current cross-coupling effect," *2014 IEEE Conference and Expo Transportation Electrification Asia-Pacific*, Beijing, 2014, pp. 1-6.
[30] H. Ge, B. Bilgin and A. Emadi, "Global loss minimization control of PMSM considering cross-coupling and saturation," *2015 IEEE Energy Conversion Congress and Exposition*, Montreal, QC, 2015, pp. 6139-6144.

**Chao Gong** was born in Shandong province in P.R. China, on February 22, 1991. He received the B.Eng. and the M.Eng degree in electrical engineering from Northwestern Polytechnical University, Xi'an, China, in 2014 and 2016, respectively. Currently, he is a PHD student in the University of Liverpool.

His research interests include electrical machines design and drives, power electronics and motion control.

**Yihua Hu** (M'13-SM'15) received the B.S. degree in electrical motor drives in 2003, and the Ph.D. degree in power electronics and drives in 2011. Between 2011 and 2013, he was with the College of Electrical Engineering, Zhejiang University as a Postdoctoral Fellow. Between 2013 and 2015, he worked as a Research Associate at the power electronics and motor drive group, the University of Strathclyde. Currently, he is a Lecturer at the Department of Electrical Engineering and Electronics, University of Liverpool (UoL). He has published 65 papers in IEEE Transactions journals. His research interests include renewable generation, power electronics converters & control, electric vehicle, more electric ship/aircraft, smart energy system and non-destructive test technology. He is the associate editor of IET Renewable Power Generation, IET Intelligent Transport Systems and Power Electronics and Drives.

**Guipeng Chen** (M'18) received the B.E.E. degree in electrical engineering from Zhejiang University, Hangzhou, China, in 2011, and the Ph.D. degree in power electronics and electric drives from the College of Electrical Engineering, Zhejiang University, in 2017. During the PHD study, he joined Fuji Electric Matsumoto Factory as a summer intern in 2014 and was invited to the University of Liverpool as a research assistant for a half-year program from July 2016. He is currently working as a Postdoc at the Instrument Science and Technology Postdoc Center, School of Aerospace Engineering, Xiamen University, China. His current research interests include automatic topology derivation of dc-dc converters and fault-tolerant converters.

**Huiqing Wen** (M'13-SM'18) received his B.S. and M.S. degrees in Electrical Engineering from Zhejiang University, Hangzhou, China, in 2002 and 2006, respectively. In 2009, he received his Ph.D. in Electrical Engineering from the Chinese Academy of Sciences, Beijing, China. From 2009 to 2010,he has been an electrical engineer working with the GE (China) Research and Development Center Company, Ltd., Shanghai, China. From 2010 to 2011, he was an engineer at the China Coal Research Institute, Beijing, China. From 2011 to 2012, he was a postdoctoral fellow at the Masdar Institute of Science and Technology, Abu Dhabi, United Arab Emirates. In 2013, he joined the Electrical and Electronic Engineering Department of Xi'an Jiaotong-Liverpool University (XJTLU), Suzhou, China. Currently, he is a senior associate professor at the XJTLU. He has published more than 100 peer reviewed technical papers in leading journals/conferences and holds over 20 issued/pending patents. His research interests include renewable energy, electric vehicle, power electronics, Microgrid, and power semiconductor devices. He is the associate editor of IEEE ACCESS, International Journal of Photoenergy, and Journal of Power Electronics.

**Zheng Wang** (S'05–M'09-SM'14) received the B.Eng. and M.Eng. degrees from Southeast University, Nanjing, China, in 2000 and 2003, respectively, and the Ph.D. degree from The University of Hong Kong, Hong Kong, in 2008, all in electrical engineering.

From 2008 to 2009, he was a Postdoctoral Fellow in Ryerson University, Toronto, ON, Canada. He is currently a full Professor in the School of Electrical Engineering, Southeast University, China. His research interests include electric drives, power electronics, and distributed generation. He has authored or coauthored over 80 internationally refereed papers and four books in these areas.

Prof. Wang received several academic awards including IEEE PES Chapter Outstanding Engineer Award, Best Paper Award of International Conference on Electrical Machines and Systems (ICMES), Best Session Paper Award of IEEE Annual Meeting of Industrial Electronics (IECON), and Nanjing Outstanding Paper Award of Natural Science.

**Kai Ni** (S'17) was born in Jiangsu, China. He received the B.Eng. (Hons) degrees in Electrical Engineering and Automation from Xi'an Jiaotong Liverpool University, Suzhou, China, and Electrical Engineering from the University of Liverpool, Liverpool, UK, in 2016. He is currently pursuing the Ph.D. degree at the University of Liverpool. His research interests include operation and control of doubly-fed induction machines, power electronic converters, and power systems.